Thermoactivated cavitation induced in water by low power, continuous wave thulium-doped fiber laser

N. Korneev, P. Rodríguez-Montero, M. Durán-Sánchez, B. Ibarra-Escamilla, and E. Kuzin

Instituto Nacional de Astrofísica, Optica y Electrónica,
Luis Enrique 1, Sta. María Tonantzintla, Puebla 72840, México.

We demonstrate that by focusing in pure water the light of a CW thulium doped fiber laser tuned at a wavelength close to the 1950 nm absorption line of the water and with power of few hundreds of milliwatts, a thermoactivated cavitation bubble formation is obtained. On collapse, a strong ultrasound wave is observed. This effect can be potentially useful for biomedical applications.

Keywords: Cavitation; fiber lasers; bioacoustics; laser-generated ultrasound.

1. Introduction

The ability of pulsed lasers to produce cavitation in water is well known [1-3]. For instance, pulsed Holmium and Thulium fiber lasers have been used in the last two decades in laser lithotripsy (destruction of kidney stones). For this application, the typical laser pulse energies are 0.5-1.0 J with pulse durations of 350 μs, for Holmium lasers [4,5]; while for Thulium fiber lasers these values range 5-75 mJ, and 200-1000 μs [5,6]. For the case of illumination with Thulium fiber lasers, cavitation bubbles with diameter up to ≈ 600 μm are formed, which on collapse produce a shock wave contributing to stone ablation [6]. This phenomenon has been employed also to study the phase transitions in liquids which take place upon pulsed laser irradiation [7,8]. More recently, it was shown that cavitation can be induced with low power continuous wave lasers also [9-12]. In this latter technique, the focused laser beam with power in the range $\sim 100 - 1000$ mW illuminates a strongly absorbing liquid (typical absorption length 0.1 mm).

The difference between the two techniques can be described as follows. From the heat transfer equation, the characteristic time after which thermal conduction becomes important is [13] $t \approx d^2/k$ (d is the size of the optical zone and k is the thermal diffusivity). For water, $k \approx 0.143$ mm^2/s, and considering an optical zone $d = 0.1$ mm (similar to the water absorption length), this characteristic time is estimated as $t \approx 7 \times 10^{-2}$ s. For pulsed lasers, the overheating of the liquid is reached during the laser pulse, and nearly all of the pulse energy is transferred to the illuminated area; this means powers of the order of hundreds of Watts - or higher - for pulses with submillisecond duration [5-8]. On the other hand, when a low power (hundreds of mW), CW laser is focused in a strongly absorbing liquid, the heat conduction becomes important, and the overheated region size can be larger than the laser beam diameter. Both the time of bubble formation and the final bubble size are determined in this latter case by a complicated interplay of the illumination geometry and the absorption coefficient, and generally demonstrate some statistical variation [9-12], with repetition frequencies usually in Hz to kHz range.

On collapse, as for the pulsed regime, a strong and short ultrasound pulse is produced (typical pressure of few MPa, and pulse duration of the order of 1 μs or less). In previous experiments, dye or inorganic salt solutions (such as saturated copper nitrate saline solution) were used together with visible or near IR lasers. The application of this technique for microfluidics [14,15], and skin perforation [16,17], was proposed. It also can be potentially useful to construct a compact and safe source of high-frequency ultrasound. However, toxic or/and corrosive dyes or salts in high concentrations, which decompose in a process of cavitation, are not suitable for most of the biomedical applications. Thus, for biomedical applications, it is interesting to obtain thermoactivation directly in water. The necessary high absorption exists there for wavelengths close to 1950 nm, where pure water exhibit an absorption peak; this wavelength is within the tuning range of the thulium-doped fiber lasers. The use of optical fiber gives as an additional advantage the possibility to make a compact device which can be easily introduced in water-filled body cavities either for therapeutic or diagnostic ultrasound-based procedures.

In this paper we report the observation of thermoactivated cavitation in pure water induced by a thulium-doped fiber laser, and describe the basic properties of the resulting ultrasound wave.

2. Experimental setup

The experimental setup for cavitation bubble detection is depicted in Fig. 1. A home-made tunable thulium-doped fiber laser (TDFL) was used to generate laser emission near the 1950 nm wavelength region with a tuning range of 44 nm. This TDFL was experimentally demonstrated and characterized in Ref. 18. A thulium-doped fiber (TDF, CoreActive SCF-TM-8/125) with a length of 10 m was used as a gain medium to generate laser emission in the wavelength range of 1950 nm. The laser wavelength selection and discrete tun-
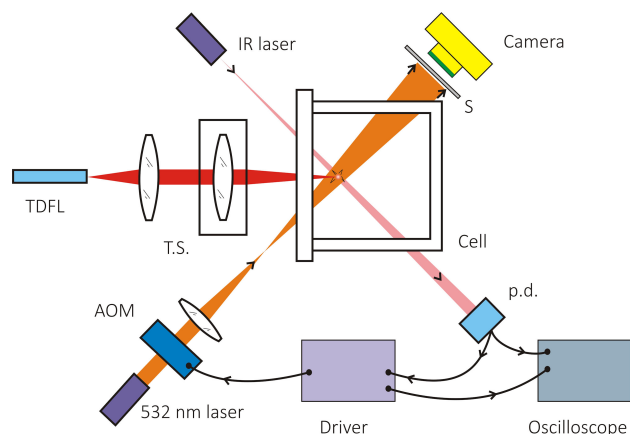
FIGURE 1. Optical setup employed for detecting cavitation bubbles induced by illumination of a low power, CW thulium-doped fiber laser (TDFL); T.S.: translation stage; p.d.: photodiode; AOM: acousto-optical modulator; S: screen.

ing was achieved by means of a high-birefringence (Hi-Bi) fiber optical loop mirror (FOLM) as spectral filter whose reflection/transmission periodically modulated spectrum is wavelength displaced by performing temperature variations on the Hi-Bi fiber loop. The output beam was collimated (with a beam diameter about 4 mm) and focused by a simple positive lens of 5 cm focal distance inside a cell filled with deionized water. To control the spot size in the cell, the focusing lens was mounted on a translation stage. The cell was $60 \times 60 \times 35$ mm in depth. Because of the high absorption of the water in this region, the formation of cavitation bubbles occurs in the vicinity of the input window. To detect the cavitation bubble, an IR diode laser beam (900 nm, 5 mW, 2 mm in diameter) passed through the incidence point of the thulium fiber laser, and it impinged on a silicon photodetector. When the bubble is formed, it acts like a short focal distance lens, causing the photodetector signal to diminish This triggers, with a suitable delay, a pulse of 70 microsecond, which opens an acousto-optical modulator for a 5 mW, 532 nm green laser beam. This latter beam is focused before the cell, and it projects an amplified image of the bubble on a screen, where the bubble shadow is recorded with a conventional camera at 1/100 s exposition.

The cavitation events produce ultrasound shock waves which are detected by a simple optical system based on the measurement of the deflection that the shock wave induces
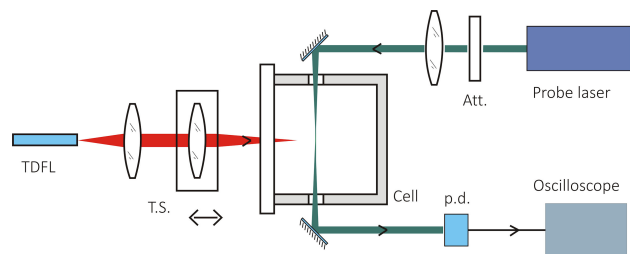

FIGURE 2. Optical setup employed to study the ultrasonic waves induced by cavitation upon illumination of a CW thulium-doped fiber laser. Att.: attenuator, and p.d.: position detector.
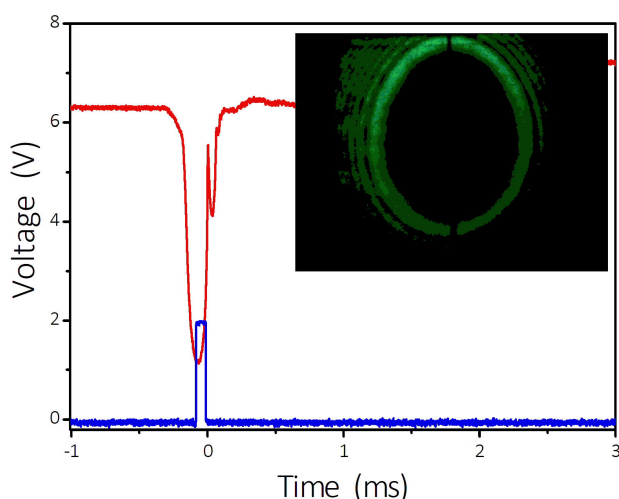

FIGURE 3. Oscilloscope traces of the photodetector signal (in red) and the modulator pulse. In the inset: photograph of the bubble projection as observed on the screen. The thin vertical line at the image center is an alignment mark on the screen.

on a focused probe laser beam, as it is shown in Fig. 2. The probe laser employed in this detection system is a CW laser with emission at 532 nm and power of 50 mW, the estimated diameter of this beam at focus was 90 μm. The beam deflection was monitored by a position detector, and the signals were displayed with a digital oscilloscope.

3. Results

The oscilloscope traces of the photodetector and modulator pulse are shown in Fig. 3; a photograph of the bubble projection is shown in the inset. It is observed that the time from the bubble formation to its collapse is around 300 microseconds, and the calculated bubble diameter is approximately 2 mm. These values are comparable to those reported for pulsed thulium and holmium fiber coupled lasers [4,6], and for thermoactivation in salt solutions [11] and pure water [12]. Note that the bubble shown in the Fig. 3 is close to the maximal size which can be obtained with our setup.

Typical ultrasonic signal is shown in Fig. 4. It was obtained near the position of the smallest spot size [see Fig. 5(a)]. It demonstrates a spike due to the first arrival of the shock wave, and some rebounds from the input window surfaces, water-air interface and cell walls. To minimize the rebounds, in this experiment the walls were covered with an ultrasound absorbing material; otherwise complicated waves propagating inside the walls arrive to the measurement spot first, resulting in speckle pattern.

The features of the obtained ultrasound signals are quite similar to those reported earlier for saturated copper nitrate saline solutions [11], which were detected by means of a hydrophone. The main characteristic results are summarized in the next figures.

Figure 5(a) shows the signal amplitude as a function of the focal spot size, as given by the water-glass interface dis-
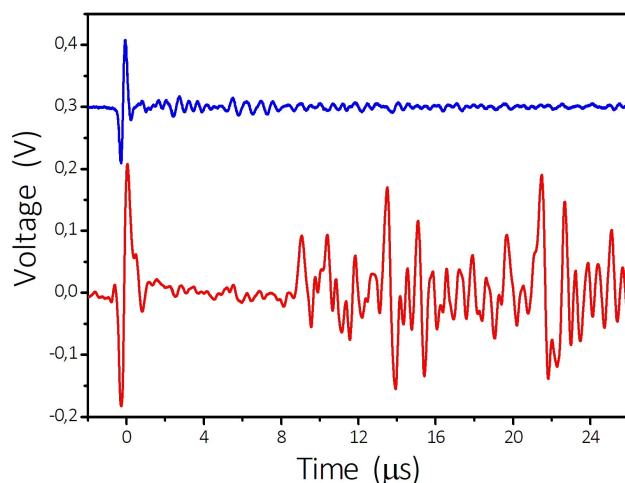
FIGURE 4. Oscilloscope trace of a ultrasonic signal produced by cavitation at the focusing lens position of -0.50 mm. The wavelength of the incident light was 1932 nm with a power of 220 mW. The triggering is done by the first spike arrival. The lower trace (in red) was obtained by the optical system, and for comparison the upper trace (in blue) was obtained with a piezoelectric transducer.

tance to the lens, for three different illuminating wavelengths (1914, 1932 and 1949 nm); while Fig. 5(b) shows the repetition frequency as a function of the focal spot size for the illuminating wavelength of 1932 nm. The power of the incident light from the TDFL on the glass window was set to 630 mW. Note that in the region 0.0 to 1.5 mm the microphone employed does not permit to detect correctly the high cavitation frequency.

Figure 6 shows the dependence of the signal amplitude and repetition frequency as a function of the incident light power near positions surrounding the position of the smallest spot size for a wavelength of 1932 nm. Note that the minimal necessary power to start the cavitation process proved to be $\approx$ 175 mW in our experimental conditions.

4. Discussion

The cavitation phenomenon presented in these experiments is qualitatively very similar to that observed in a solution of inorganic salt reported in Ref. [11]. The characteristic frequencies, amplitude dependences and necessary laser powers correspond well to those observed earlier for solutions and for water illuminated at 1.9 μm [12].
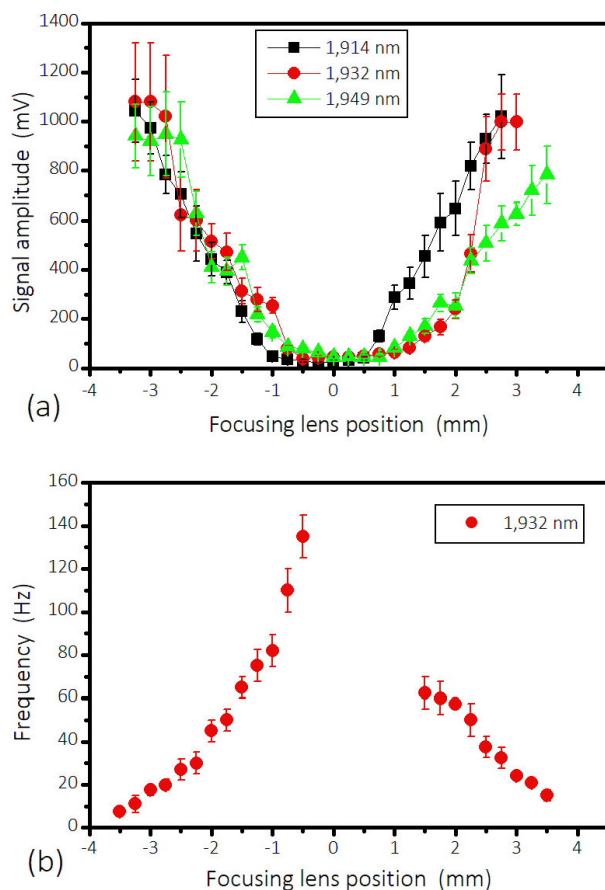

FIGURE 5. Signal amplitude (a) and repetition frequency (b) as a function of the focal spot size, as given by the focusing lens position. The zero position corresponds to the beam focused at the water-glass interface. The incident light power was 630 mW.
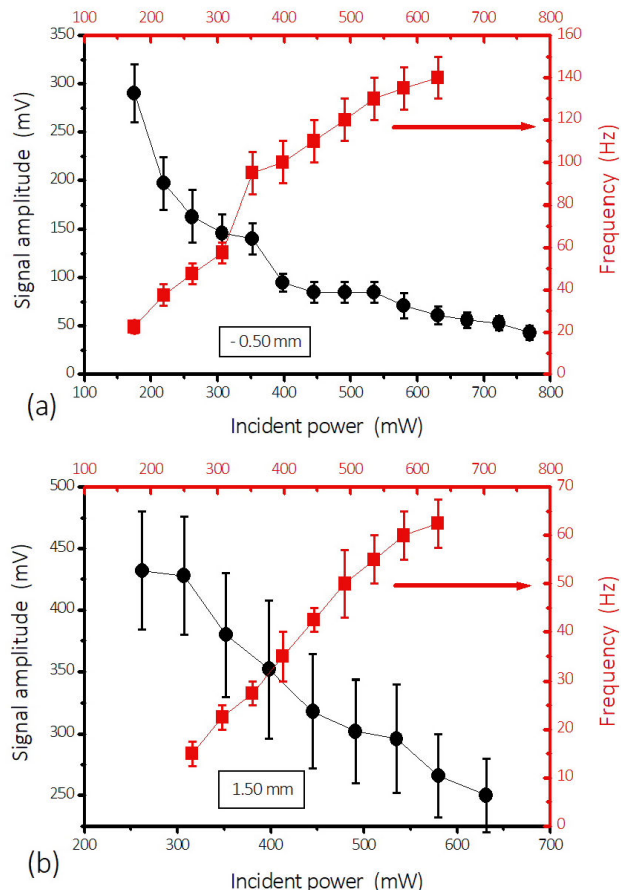

FIGURE 6. Signal amplitude and repetition frequency as a function of the incident light power at two different positions surrounding the position of minimal spot size (a) at -0.50 mm and (b) at 1.50 mm positions. The illuminating wavelength was 1932 nm.

From Fig. 5(b) it is observed that the pulse repetition frequency is maximal for the exact focus (close to the 0.0 mm position), and it diminishes when the laser spot becomes bigger, but the pulse amplitude, on the contrary, is higher for bigger laser spots [Fig. 5(a)]. So there is a critical laser spot size; when the incident beam is too large, the cavitation does not occur. It is worth noting that the interval between subsequent cavitation events varies with a wide statistical distribution [see errors bars in Figs. 5(b) and 6]; the variation in the interval is especially pronounced for large lens displacements from focus. There is a slight asymmetry (difference for a same beam spot size before and after the focus), which occurs because of slightly different geometry (converging or diverging beam inside the water). Because the absorption length is small, for a lens with a large focal distance this asymmetry is not so pronounced; it is observed more clearly in lenses with short focal distances.

These features are explained by thermoactivation mechanism [9]. For tight focusing, a small volume is overheated rapidly, thus the time between the subsequent events is short. Because of this small volume of overheated region, the cavitation bubble is small, as well as the energy stored; which results in a wave of low amplitude. In fact, for a fixed spot size (as given by the lens distance from the cell window) the pulse amplitude becomes larger for lower intensity levels (see Fig. 6), which was observed for solutions as well [11]. For a bigger illuminated volume, a bigger bubble is produced, which results in higher wave amplitude and lower repetition rate. If the illuminated volume is too big, overheating cannot be achieved, thus no cavitation is produced.

For our wavelength tuning range (1914-1949 nm), the absorption length varies less than 10% and it is approximately 0.09 mm at 1950 nm [19]. Thus, not much variation in signal is observed in function of wavelength [Fig.5(a)].

Multiple cavitation events close to the optical window finally produce damage to the glass surface in form of microscopic dents. This is especially pronounced for ultrasonic waves with large amplitudes and low repetition frequency produced by large laser spots. The damage to the glass can finally distort the input beam up to the point where cavitation stops, but it can be resumed by moving the beam to a fresh point. The cavitation can also be induced by placing the fiber output end directly into the water [12]. However, after a few cavitation events, the fiber output end is affected mechanically as well.

It is interesting to compare CW and pulsed laser regimes for cavitation bubble formation. For thermoactivation mechanism the power of the CW lasers is much lower than the instantaneous power of the pulsed ones (up to two orders of magnitude), and the maximal repetition rate is higher (hundreds of Hz compared with tens of Hz for pulsed lasers). The maximal ultrasound wave amplitude obtained with CW illumination, as estimated by the bubble size, is similar to that obtained for laser lithotripsy, but the direct laser ablation, which is important also [4,7], is much smaller due to lower average laser power. Generally, the action of thermoactivated and pulse-induced cavitation on biological tissues can be quite different and further investigation is needed. Here we limit ourselves to the demonstration of principle.

The choice of the visualization technique was affected by the available equipment. Most probably images with better quality can be obtained with incoherent stroboscopic illumination, or by a high-speed camera, as reported, for instance, in Refs. 11 and 12 . However, we consider that the resulting image quality is sufficient to estimate the bubble size. Our results, as expected, are very similar to those obtained for water with dyes at other illumination wavelengths [12]. The main contribution of this report is the experimental demonstration of the possibility to work with pure water by the appropriate choice of the wavelength.

5. Conclusions

We have demonstrated that cavitation can be obtained in water using low power CW laser with a wavelength close to 1950 nm, and that the features of the resulting cavitation are quite similar to those obtained for inorganic salt solutions with similar absorption at visible and NIR wavelengths. Different from the effects produced by pulsed lasers systems, thermoactivation mechanism can produce higher repetition rates with smaller bubbles; the bigger bubbles generated by thermoactivation have a size comparable to those obtained with pulsed lasers systems. However, the peak laser power for thermoactivation is much smaller, which potentially can result in more compact, cheaper and safer systems.

1. A. Philipp and W. Lauterborn, *J. of Fluid Mech.* **361** (1998) 75.

2. W. Song, M. Hong, B. Lukyanchuk, and T. Chong, *J. of Appl. Phys.* **95** (2004) 2952.

3. K.-T. Byun, H.-Y. Kwak, and S. W. Karng, *Japanese J. of Appl. Phys.* **43** (2004) 6364.

4. K. F. Chan *et al.*, *Lasers in Surgery and Medicine* **25** (1999) 22.

5. N. M. Fried, *Lasers in Surgery and Medicine* **37** (2005) 53.

6. L. A. Hardy, J. D. Kennedy, C. R. Wilson, P. B. Irby and N. M. Fried, *Proc. SPIE* **9689** (2016) 96891B.

7. A. A. Samokhin, N. N. Il'ichev, P. A. Pivovarov, and A. V. Sidorin, *Appl. Phys. A* **122** (2016) 594.

8. A. A. Samokhin, N.N. Il'ichev, P. A. Pivovarov, and A. V. Sidorin, *Bulletin of the Lebedev Physics Institute* **43** (2016) 156.

9. S. Rastopov and A. Sukhodol'sky, *Phys. Lett. A* **149** (1990) 229.

10. S. F. Rastopov and A. T. Sukhodolsky, *Proc. SPIE* **1440** (1991) 127.

11. J. Ramirez-San-Juan, E. Rodriguez-Aboytes, A. Martinez-Canton, O. Baldovino-Pantaleon, A. Robledo-Martínez, N. Korneev, and R. Ramos-García, *Opt. Express* **18** (2010) 8735. 12.

12. V. I. Yusupova, A. N. Konovalovb, V. A. Ul'yanovb, and V. N. Bagratashvilib, *Acoustical Physics* **62** (2016) 537.

13. Steven L. Jacques, *Appl. Opt.* **32** (1993) 2447.

14. A. Jian, K. Zhang, Y. Wang, S. Lau, Y. Tsang, and X. Zhang, *Sensors and Actuators A: Physical* **188** (2012) 329.

15. R. Dijkink and C.-D. Ohl, *Lab on a Chip* **8** (2008) 1676.

16. Y. Tagawa, N. Oudalov, A. El Ghalbzouri, C. Sun, and D. Lohse, *Lab on a Chip* **13** (2013) 1357.

17. C. Berrospe-Rodriguez, C. W. Visser, S. Schlautmann, R. Ramos-García, and D. Fernández Rivas, *Biomicrofluidics* **10** (2016) 014104.

18. B. Posada-Ramírez, M. Durán-Sánchez. R. I. Álvarez-Tamayo, B. Ibarra-Escamilla, Edgar Bravo-Huerta, and E. Kuzin, *Opt. Express* **25** (2017) 2560.

19. Joseph A. Curcio and Charles C. Petty, *J. of the Opt. Soc. Am.* **41** (1951) 302.